THE JOURNAL OF PHYSICAL CHEMISTRY B
A JOURNAL OF THE AMERICAN CHEMICAL SOCIETY

pubs.acs.org/JPCB

Article

Stimulated Raman Scattering Imaging Sheds New Light on Lipid Droplet Biology

Published as part of The Journal of Physical Chemistry virtual special issue "Xiaoliang Sunney Xie Festschrift".

Hao Jia and Shuhua Yue*

Cite This: *J. Phys. Chem. B* 2023, 127, 2381−2394

Read Online

ACCESS | Metrics & More | Article Recommendations

ABSTRACT: A lipid droplet (LD) is a dynamic organelle closely associated with cellular functions and energy homeostasis. Dysregulated LD biology underlies an increasing number of human diseases, including metabolic disease, cancer, and neurodegenerative disorder. Commonly used lipid staining and analytical tools have difficulty providing the information regarding LD distribution and composition at the same time. To address this problem, stimulated Raman scattering (SRS) microscopy uses the intrinsic chemical contrast of biomolecules to achieve both direct visualization of LD dynamics and quantitative analysis of LD composition with high molecular selectivity at the subcellular level. Recent developments of Raman tags have further enhanced sensitivity and specificity of SRS imaging without perturbing molecular activity. With these advantages, SRS microscopy has offered great promise for deciphering LD metabolism in single live cells. This article overviews and discusses the latest applications of SRS microscopy as an emerging platform to dissect LD biology in health and disease.

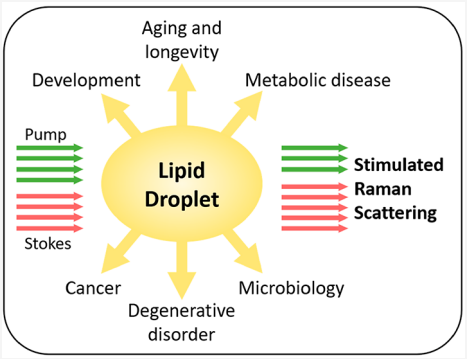

INTRODUCTION

Lipid droplets (LDs) are composed of a hydrophobic core of neutral lipids, predominantly triglycerides (TGs) and cholesteryl esters (CEs), encircled by a phospholipid monolayer with various LD-associated proteins.[1] As a hub in cellular metabolism, LDs act as reservoirs for excess fatty acids and cholesterol, which can be released for energy production, membrane synthesis, and signaling when needed, to maintain metabolic homeostasis and support cellular processes.[2] LD dysregulation has been frequently observed in human diseases, including development, aging and longevity, metabolic diseases, cancers, degenerative disorder, microbiology, and so on. Therefore, it is essential to improve the understanding of the role of LDs in physiology and pathology.

An LD is a highly dynamic organelle that needs to balance deposition and mobilization of diverse lipid species to maintain crucial cellular functions. Despite their ubiquitous presence, the number, size, and composition of LDs vary remarkably from one to anther and change dynamically along with various cellular processes.[3] An LD pool within a single cell consists of distinct LD subpopulations with different distribution and composition, which may contribute to cellular lipid homeostasis.[4,5] Such dramatic spatiotemporal heterogeneity of LDs highlights an urgent need to develop novel analytical methods with high spatiotemporal resolution to study LD biology *in situ*.

Traditionally, LDs are visualized through staining with hydrophobic dyes or fluorescent probes, which lacks compositional information. For analysis of lipid composition, mass spectrometry and nuclear magnetic resonance spectroscopy are commonly used but lack spatial information. Mass spectrometry imaging has been developed to map the distribution of various lipid species *in situ* but cannot study live biological samples because of invasive nature and could hardly analyze individual LDs due to limited spatial resolution.[6,7] As an alternative, Raman scattering offers the contrast specific to molecules from vibrations of chemical bonds in a label-free manner.[8−10] Owing to high chemical selectivity, subcellular spatial resolution, and noninvasiveness, spontaneous Raman microscopy has been used to examine the intracellular lipids in single cells.[11,12] Particularly, Raman imaging of lipids has demonstrated a great advantage over the use of fluorescence because the label-free manner preserves the hydrophobicity of the lipid molecule, which essentially underlies all aspects of lipid biology. Unfortunately, due to weak signals, spontaneous

Received: January 3, 2023
Revised: February 5, 2023
Published: March 10, 2023

https://doi.org/10.1021/acs.jpcb.3c00038
J. Phys. Chem. B 2023, 127, 2381−2394

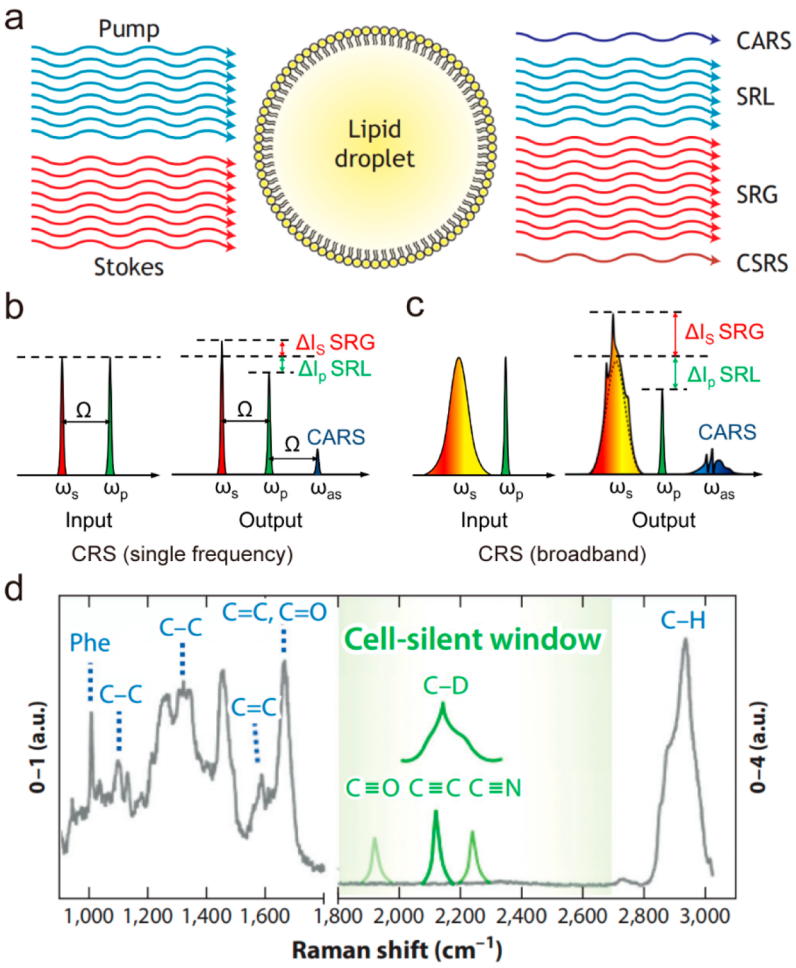

Figure 1. Stimulated Raman scattering (SRS) imaging of lipid droplets (LDs). (a) Principle of coherent Raman scattering (CRS). In CRS, the synchronized pump and Stokes photons can generate enhanced anti-Stokes fluorescence and transfer energy between each other mediated by the molecules. CARS, coherent anti-Stokes Raman scattering; SRL, stimulated Raman loss; SRG, stimulated Raman gain, CSRS, coherent Stokes Raman scattering. (b) Two narrowband lasers generate single-frequency CRS. (c) A narrowband laser and a broadband laser simultaneously excite multiple Raman transitions. ω_p, ω_s, and ω_{as}, denote the frequencies of the pump, Stokes beam, and anti-Stokes beam, respectively; Ω is the fundamental. (d) Two types of vibrational contrast are explained on a Raman spectrum. Gray line shows the typical Raman spectrum of a HeLa cell from 900 cm^{-1} to 3,000 cm^{-1} wavenumbers. Intrinsic contrast originates from the vibration of intrinsic chemical bonds (blue). Vibrational tags (green) show distinct Raman bands in the cell-silent window. Panel a adapted with permission from ref 22. Copyright 2022 The Company of Biologists. Panels b and c adapted with permission from ref 16 . Copyright 2015 AAAS. Panel d adapted with permission from ref 47. Copyright 2019 Annual Reviews.

Raman microscopy has limited imaging speed, which hinders its application in LD research. Taken together, without enough information regarding spatial and temporal dynamics, these methods have difficulty elucidating how exactly the LDs are formed and metabolized, and how they function in single live cells.

In order to address the problem of slow imaging speed in spontaneous Raman microscopy, coherent Raman scattering (CRS) microscopy has been developed by extraordinarily enhancing Raman signals.[13−16] As shown in Figure 1a, when the frequency difference between the pump beam (ω_p) and the Stokes beam (ω_s) is resonant to the vibration frequency of a molecule, four major CRS processes occur simultaneously, namely coherent anti-Stokes Raman scattering (CARS), stimulated Raman loss (SRL), stimulated Raman gain (SRG), and coherent Stokes Raman scattering (CSRS). Both SRL and SRG belong to a stimulated Raman scattering (SRS) process. As nonlinear optical processes of coherent excitation, vibrational activation rates of CRS can be drastically accelerated by 10^8 that of the inherently weak spontaneous Raman scattering. The large signal level of CRS microscopy enables it to achieve fast imaging speed, which makes real time imaging available for living biological systems. CARS is a vibrationally enhanced four-wave mixing process, and the signal is generated at a new frequency apart from input beams. Although CARS microscopy has promoted the study of LD biology in the past two decades,[8,17−20] its nonresonant background limits applications to some extent. Specifically, the nonresonant background leads to distortion of the CARS spectrum relative to the spontaneous Raman spectrum of the target biomolecule, which not only complicates the quantification process but also makes it difficult to image biomolecules specifically. In addition, for weaker Raman bands, the CARS signal is often buried in a large nonresonant background contributed by the medium. To further enhance sensitivity and specificity, SRS microscopy was developed in 2008 and for the first time applied to label-free biomedical imaging.[21] In contrast to CARS, the SRS signal is intrinsically free of

https://doi.org/10.1021/acs.jpcb.3c00038
J. Phys. Chem. B 2023, 127, 2381−2394

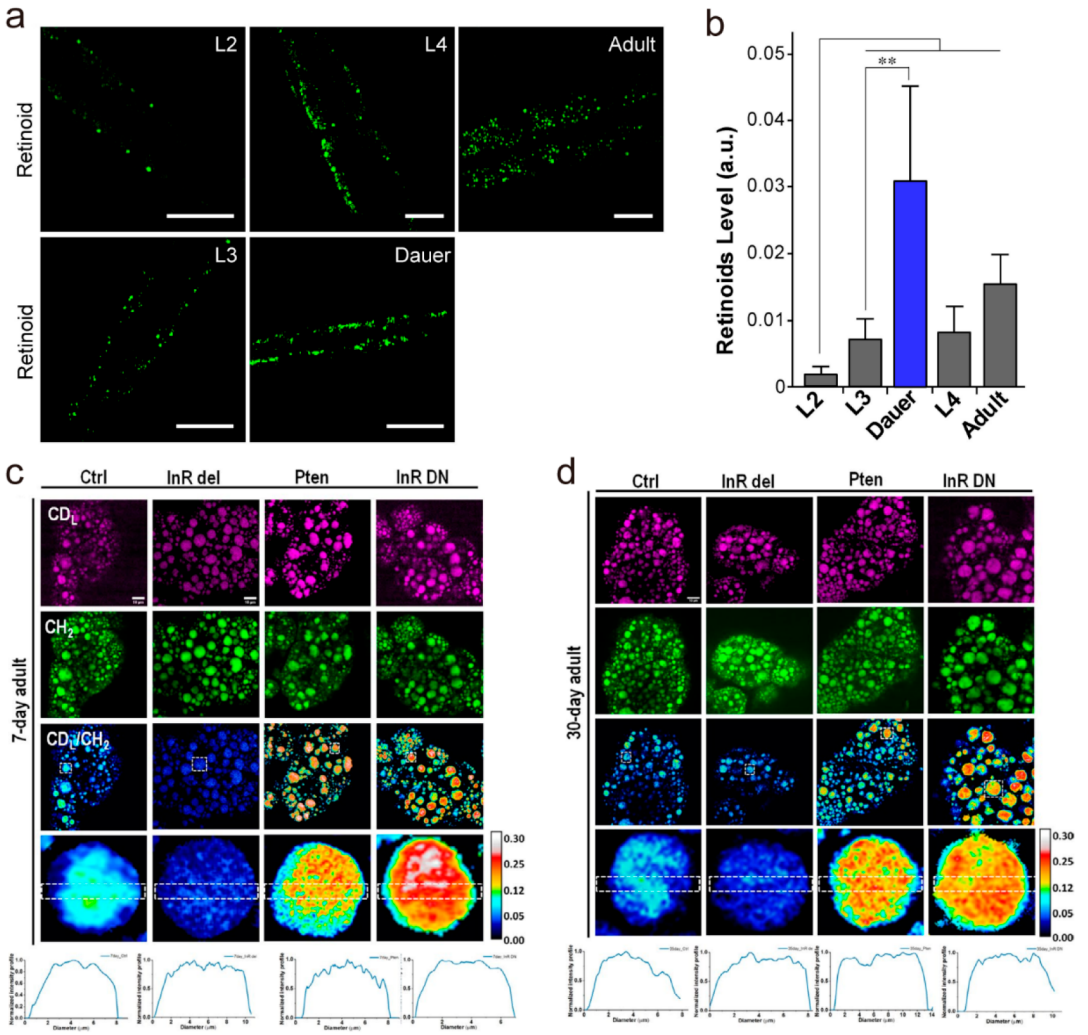

Figure 2. Stimulated Raman scattering (SRS) imaging of lipid droplets (LDs) in development, aging, and longevity. (a) SRS (1580 cm^{-1}) imaging of retinoids in WT L2, L4, and adult worms and dauer induced from *daf-2(e1370)*. Scale bar: 20 μm. (b) Quantitative analysis of retinoids in panel a, * denotes $P \leq 0.05$. (c, d) DO-SRS imaging of lipid metabolism in the fat body of mutant flies at (c) 7-day and (d) 30-day posteclosion. The ratiometric images (CD_L/CH_2) display the ratio of CD signal at 2143 cm^{-1} (newly synthesized lipids) to the signal at 2850 cm^{-1} (CH_2 stretching of lipids). The genetic downregulation of the InR/PI3K pathway (Pten, ppl-Gal4 > UAS-Pten; InR DN, ppl-Gal4 > UAS-InR DN) showed higher lipid metabolism than control, and upregulation of the InR/PI3K pathway (InR del, ppl-Gal4 > UAS-InR del) led to reduced lipid metabolism in both young and old flies. Scale bar: 10 μm. Panels a and b adapted with permission from ref 59. Copyright 2018 European Chemical Societies Publishing. Panels c and d adapted with permission from ref 66 licensed under https://creativecommons.org/licenses/by/4.0/.

nonresonant background and provides spectral profiles that are nearly identical to spontaneous Raman spectrum. Moreover, the SRS intensity is linearly dependent on molecular concentration, which enables straightforward interpretations of chemical mapping to generate quantitative concentration maps of targeted biomolecules. Since then, SRS microscopy has been widely used to improve current understanding of the role of LD in health and disease.

We note that technical developments and biological applications of SRS microscopy have been extensively discussed in multiple reviews.[22−25] Here, we will focus on the applications of SRS microscopy to understanding LD biology in various physiological and pathological conditions.

SRS Microscopy: Technical Advancements Favorable for LD Analysis. The first implementation of SRS microscopy was reported in 2008.[21] Since then, SRS microscopy has been widely used for visualization of specific biomolecules, such as lipids, nucleic acids, and proteins inside single live cells. For example, by tuning the pump wavelength to be resonant with the CH_2 band at 2850 cm^{-1}, SRS signals arose mainly from intracellular LDs. Thus, with high spatiotemporal resolution, label-free SRS microscopy has been applied not only to map the distribution but also to monitor the dynamics of LDs in living cells and organisms.[26−29] However, single-color SRS that can only obtain morphological information on LDs has limited capability to quantitatively analyze multiple chemical compositions.

To quantitatively measure multiple components with overlapping Raman bands, multicolor SRS microscopy (e.g., two-color and three-color SRS microscopy) has been developed by tuning laser wavelengths to match multiple vibrational frequencies.[30−32] Based on linear decomposition of the multicolor SRS images, several molecular signatures can be obtained simultaneously, for instance including CH_2, CH_3, and =C−H vibrational bands which represent total lipids, proteins, and unsaturated lipids, respectively.[33−35] Never-

https://doi.org/10.1021/acs.jpcb.3c00038
J. Phys. Chem. B 2023, 127, 2381−2394

theless, it remains difficult for multicolor SRS microscopy to resolve complex biological components.

To address this challenge, hyperspectral SRS and multiplex SRS microscopy have been developed to unravel chemical species in complex biological environments. The spectra acquired by hyperspectral or multiplex SRS can cover the C−H or fingerprint vibrational regions, providing rich molecular information (Figure 1b,c). Hyperspectral or multiplex SRS can be implemented with a narrowband and a broadband laser by different detection manners[36−39] or two chirped broadband lasers by spectral focusing.[40−42] These modalities offer the potential for providing more abundant chemical information on subcellular compartments, which are desirable for use to investigate the heterogeneous distribution of LDs with different compositions across different systems, track the dynamic interactions between LDs and other organelles, elucidate the underlying metabolic signaling pathways, and ultimately uncover novel diagnostic marker or therapeutic target for diseases.

To further enhance sensitivity and specificity, a variety of Raman tags have been incorporated into SRS microscopy. Small-size Raman tags, with distinct and strong Raman peaks well separated from endogenous cellular background, offer a great opportunity to increase molecular selectivity and improve detection sensitivity of SRS microscopy without perturbing biological activities of small biomolecules (Figure 1d). The commonly used Raman tags include stable isotopes (e.g., deuterium and ^{13}C) and biorthogonal tags (e.g., alkyne, nitrile, diyne).[43−48] SRS imaging of Raman tags has been used to study LD accumulation,[49] *de novo* synthesis, and exogeneous uptake as the source of lipids stored in LDs.[50,51] Together, SRS microscopy incorporated with small Raman tags has opened new doors for the study of LD biology.

Taking advantage of the above technical advancements, SRS microscopy has shed new light on LD biology in development, aging and longevity, metabolic disease, cancer, degenerative disorder, and microbiology, which are reviewed as below.

SRS Imaging of LDs in Development. LD plays an essential role in embryo development. During preimplantation development, early mammalian embryos have been reported to actively uptake, synthesize, and accumulate lipids in LDs.[52−54] In contrast, only scarce LDs are found in early post-implantation embryonic tissues,[55] implying active mobilization of LDs during the transition from naive to primed pluripotent states. LDs vary in size and number in different species and also at different developmental stages. Whereas LDs in mouse oocytes at germinal vesicle and metaphase II stages and embryos at early developmental stages (2-, 4-cell embryos) are of a uniform small size, LDs in cells of the 8-cell blastocyst-embryo stage are heterogeneous and large in size.[56] LD distribution also reflects the metabolic state of oocyte and embryo; that is, a wide dispersion of LDs appears to be associated with increased β-oxidation at an early developmental stage while fusion of LDs coincides with glycolysis at the morula stage.

With chemical specificity, SRS microscopy has been used to detect the LD dynamics during development. Based on SRS microscopy, Dou et al. developed a mathematical model of velocity-jump process to simulate LD bulk displacement during early embryogenesis, which will improve our quantitative understanding of many mechanisms during development.[57] By integrating SRS microscopy with gene screening, Han et al. unveiled that C13C4.5, a negative gene regulator of lipid content, could interferewith lysosome morphology and function by changing the size and fat content of LDs, thus regulating the number of offspring in *C. elegans*.[58]

Besides size and amount, composition of LD also impacts development. Particularly, retinoids stored in LDs play crucial roles in lipid metabolism and development. Due to the small molecule size that limits labeling with bulky fluorescent dyes, retinoids are invisible to conventional fluorescence microscopy. To address this problem, Chen et al. developed a label-free hyperspectral SRS microscope to map retinoids inside LDs based on molecular signatures in the fingerprint region. Enabled by this method, the authors discovered that spatiotemporal dynamic storage of retinoids in *C. elegans* is tightly associated with developmental stages.[59] Specifically, retinoid levels increase with developmental time, and surprisingly exhibit a dramatic induction in dauer larvae (Figure 2a,b), suggesting that retinoid accumulation is a general phenomenon associated with dauer formation and maintenance but not restricted to a specific dauer inducing mechanism.

Collectively, owing to its high sensitivity, negligible photodamage, and label-free capability, SRS microscopy currently permits quantitative analysis of content, composition, and distribution of highly dynamic LDs throughout oocyte maturation and embryonic development. Nevertheless, the comprehensive crosstalk and mechanisms of lipid metabolism from maternal and embryonic origin remain unclear.[54] In the future, we expect that SRS microscopy can make more contributions to deeper understanding of lipid metabolism in the physiological context of early embryo development, which may further improve early embryo survival.

SRS Imaging of LDs in Aging and Longevity. As most organisms age, the metabolism slows down, which results in a gradual accumulation of neutral lipid in LDs.[60] Such LD accumulation has been shown to protect aging cells against cold stress.[61] Besides, biosynthesis and mobilization of LDs are also associated with longevity regulation.[62] The increased LD mobilization promotes a metabolic shift toward fatty acid β-oxidation, which has been linked with longevity mechanisms.[63]

SRS microscopy allows quantitative study of LD mobilization during aging and longevity. By using SRS microscopy and other molecular biology analytical methods, Ramachandran et al. demonstrated that the induction of specific lysosomal signaling, mediated by a LIPL-4 lysosomal acid lipase and its lipid chaperone LBP-8, increases mitochondrial β-oxidation, which further reduces LD storage and promotes longevity in *C. elegans*.[64] The authors discover a crucial role for lysosomal lipid messenger signaling to actively trigger adjustments in mitochondrial activity that in turn coordinates lipid metabolism, redox homeostasis, and longevity. By integrating heavy water (D_2O) probing with SRS (DO-SRS) microscopy, Li et al. directly visualized metabolic activities in the fat body of *Drosophila* melanogaster during aging *in situ*.[65,66] The authors discovered a dramatic decrease in lipid turnover in 35-day-old flies. In contrast, the decrease of the protein turnover rate occurred earlier than for the lipid (25-day vs 35-day); moreover, they observed many proteins localized on the cell and LD membrane, suggesting that protein metabolism may play an important role as a prerequisite for the changing lipid metabolism during the aging process.[65] They subsequently found that calorie restriction, low protein diet, and (moderately) high protein and high sucrose diets enhanced lipid turnover in flies at all ages, while (moderately) high

https://doi.org/10.1021/acs.jpcb.3c00038
J. Phys. Chem. B 2023, 127, 2381−2394

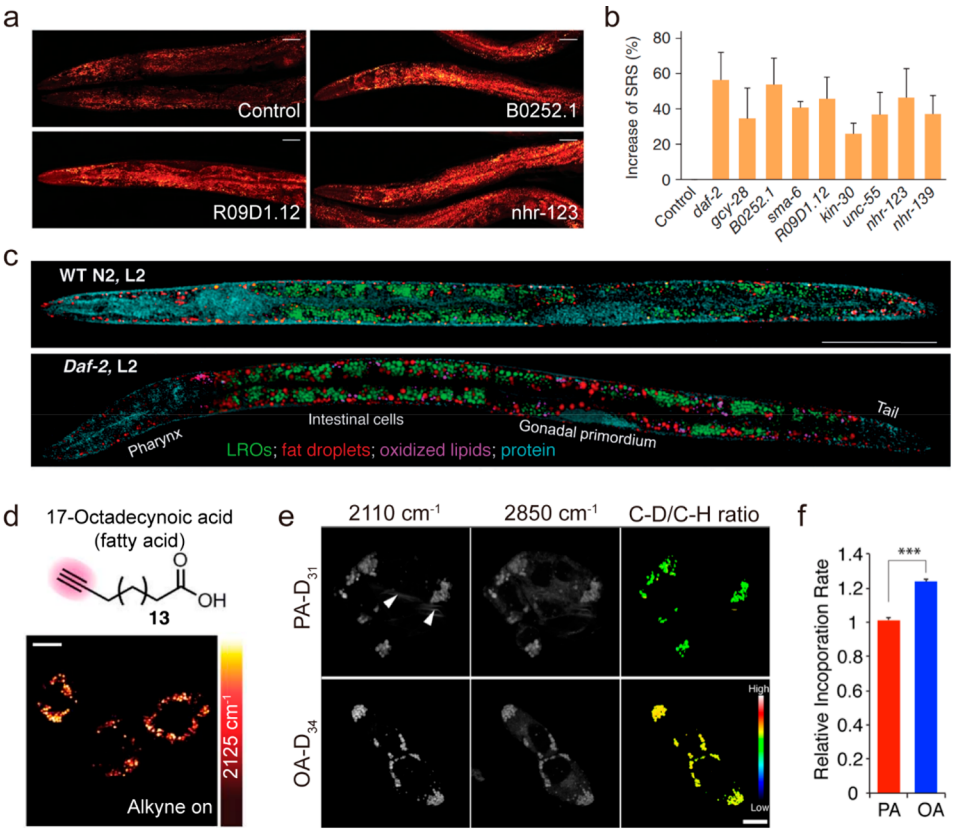

Figure 3. Stimulated Raman scattering (SRS) imaging of lipid droplets (LDs) in metabolic diseases. (a, b) RNAi screening of new fat storage regulatory genes based on *in vivo* lipid quantification using label-free SRS microscopy. (a) SRS images of three candidate worms and the control group. Control, worms fed with bacteria containing empty vectors. Scale bars, 50 μm. (b) SRS signal increase compared to the control for genes that resulted in a fat content increase of more than 25% when inactivated by RNAi ($P < 0.0001$, $n = 5$ worms). All the experiments were performed twice independently. Results from one experiment are shown. Error bars, s.d. (c) Compositional analysis of intracellular compartments in whole *C. elegans* worms by hyperspectral SRS imaging. MCR concentration maps of neutral fat droplets, lysosome-related organelles (LROs), oxidized lipids, and protein in the body of whole wild-type worms and daf-2 mutants. Scale bar: 50 μm. (d) Live macrophages incubated with 400 μM 17-octadecynoic acid (alkyne on). Scale bar: 10 μm. (e, f) Tracking incorporation dynamics of different fatty acid molecules in hepatic cells with deuterium-labeling-coupled hyperspectral SRS. (e) Hyperspectral SRS images of hepatic cells (McA-RH7777) labeled with either PA-D_{31} or OA-D_{34} for 7 h. The incorporation of deuterated fatty acids was imaged at 2110 cm^{-1}, and the total lipid level was imaged at 2850 cm^{-1}. The ratio between the C−D and the C−H signal intensities was used to measure the level of fatty acid incorporation into LDs. Arrowheads indicate abnormal membrane-like structures caused by PA feeding. Scale bar = 10 μm. (f) The incorporation rate of OA-D_{34} is 24% faster than PA-D_{31} in hepatic cells. $n = 93$ for PA-D_{31}; $n = 244$ for OA-D_{34}. ***$p < 0.001$. Panels a and b adapted with permission from ref 71. Copyright 2011 Springer Nature. Panel c adapted with permission from ref 74. Copyright 2014 Wiley. Panel d adapted with permission from ref 73. Copyright 2014 Springer Nature. Panels e and f adapted with permission from ref 26. Copyright 2014 American Chemical Society.[73]

fructose and glucose diets only promoted lipid turnover in aged flies. Meanwhile, downregulating the insulin signaling pathway enhanced lipid turnover, which is likely related to lifespan increase, while upregulating insulin signaling pathway decreased lipid turnover that would shorten the lifespan. These results investigated the impacts of diet composition on lipid metabolism and life span, as well as the insulin pathway on lipid metabolism, for a better understanding of the roles lipid metabolism plays in aging and life span[66] (Figure 2c,d).

Although lipid metabolism potently regulates aging and lifespan, the lipid metabolic dynamics during the aging process is still unclear. SRS microscopy enables direct visualization and quantification of the spatiotemporal changes of LDs as well as metabolic turnover of other biomolecules in live animal *in situ* at the subcellular level, providing a better understanding of the impact of LD homeostasis on aging and longevity. In the future, we expect SRS microscopy will focus more on aging and age-related diseases in live animals *in situ*, which may contribute to better understanding of the molecular mechanism underlying aging and more discovery of novel health-promoting and lifespan-extending lipid metabolic targets.

SRS Imaging of LDs in Metabolic Diseases. LD accumulation has been recognized as a hallmark of various metabolic diseases, including obesity and atherosclerosis.[67,68] Obesity is a state of excess lipid storage in LDs of adipose tissues, or even nonadipose tissue. The excessive LD accumulation may cause lipotoxicity or tissue dysfunction. Like obesity, atherosclerosis is associated with excessive deposition of lipids in tissues; in this instance, CEs are stored in LDs until they can be mobilized. Therefore, it is essential to understand the biological mechanisms and clinical implications of LD accumulation in metabolic diseases.

Obesity can be commonly characterized as a disorder in LD homeostasis. Thus, research on the identification of LD dysregulation could greatly facilitate the prevention and treatment of obesity. To this end, *C. elegans* is a great model for exploring LD storage.[69] Like mammals, *C. elegans* store lipids in LDs, and the synthesis and degradation pathways of

https://doi.org/10.1021/acs.jpcb.3c00038
J. Phys. Chem. B 2023, 127, 2381−2394

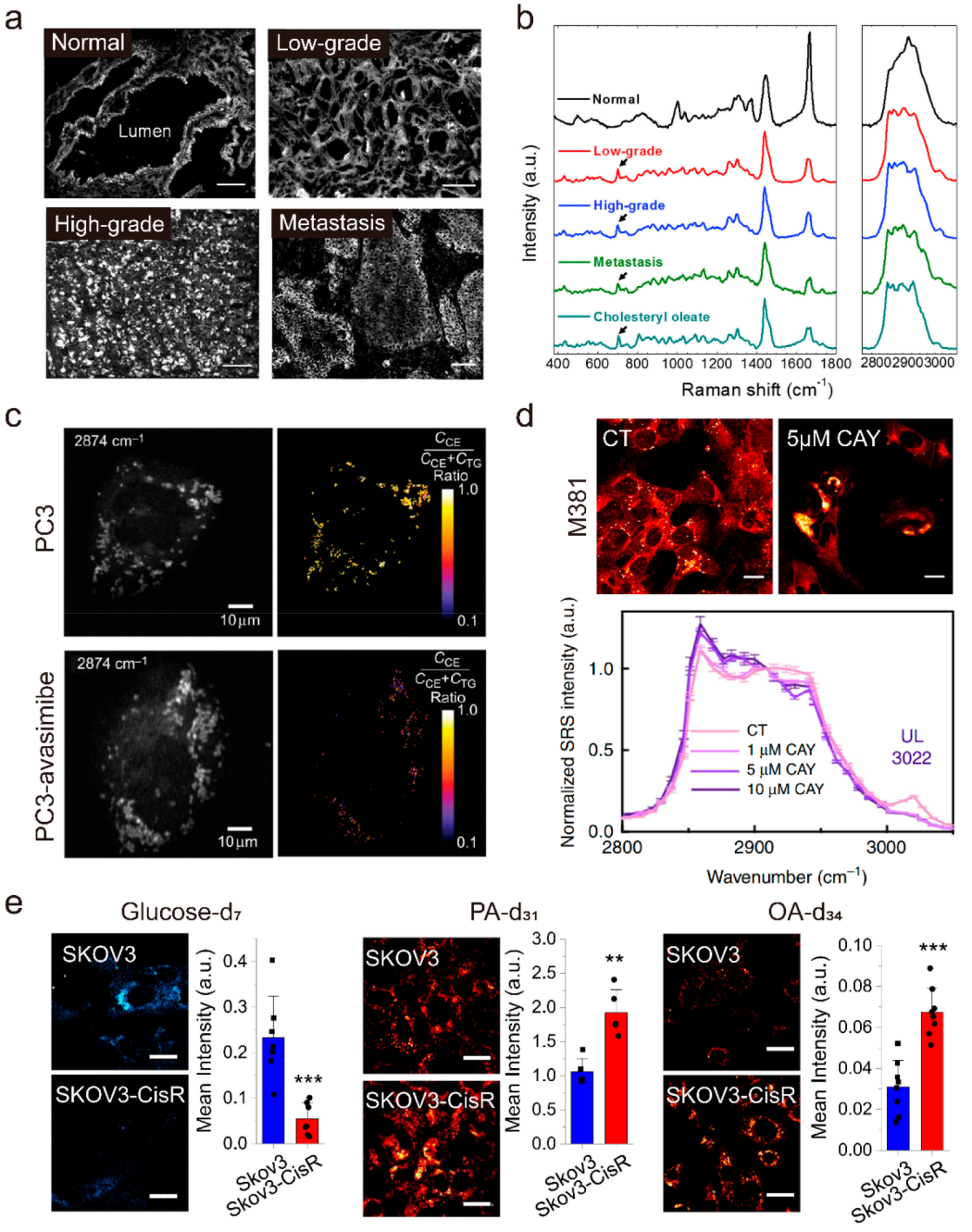

Figure 4. Stimulated Raman scattering (SRS) imaging of lipid droplets (LDs) in cancer research. (a, b) Aberrant cholesteryl ester accumulation in human prostate cancer (PCa) tissues. (a) SRS images of benign prostate, low-grade PCa, high-grade PCa, and metastatic PCa (liver), respectively. Scale bar, 100 μm. (b) Raman spectra of autofluorescent granules in normal prostate, LDs in PCa, and pure cholesteryl oleate. Spectral intensity was normalized by CH_2 bending band at 1442 cm^{-1}. Black arrows indicate the bands of cholesterol rings at 702 cm^{-1}. (c) SRS image of single live PC3 cells or avasimibe-treated PC3 cells at 2874 cm^{-1} and the corresponding cholesteryl ester (CE) percentage map. Scale bar, 10 μm. TG, triglyceride. (d) Representative lipid channel SRS images from the same set of M381 cells in control (CT) or 5 μM CAY treatment. Normalized (to 2908 cm^{-1}) hyperspectral SRS spectra of LDs in M381 cells without (CT) and with treatment of 1, 5, and 10 μM CAY for 3 days. Scale bar, 20 μm. (e) Representative SRS images of SKOV3 and SKOV3-cisR cells fed with glucose-d_7 for 3 days, palmitic acid-d_{31} (PA-d_{31}) for 6 h, or oleic acid-d_{34} (OA-d_{34}) for 6 h and quantitative analysis of SRS signal of C−D bonds by mean intensity, respectively. Scale bar, 20 μm. Panels a and b adapted with permission from ref 87. Copyright 2014 Elsevier. Panel c adapted with permission from ref 39. Copyright 2015 Springer Nature. Panel d adapted with permission from ref 98 licensed under https://creativecommons.org/licenses/by/4.0/. Panel e adapted with permission from ref 100 licensed under https://creativecommons.org/licenses/by/4.0/.

lipid molecules are highly conserved.[70] In addition, the whole-body transparency of *C. elegans* throughout all life stages allows most optical microscopies for phenotyping at cell, tissue, and organism levels. Taking advantage of SRS microscopy in lipid imaging, a reverse genetic screen was conducted in *C. elegans*, searching for genes regulating LD accumulation.[71] Out of 36 receptor tyrosine kinases (RTKs) and 236 nuclear hormone receptors (NHRs), eight genes were identified whose inactivation increases LD content levels (Figure 3a,b), suggesting SRS imaging is a reliable and quantitative method

https://doi.org/10.1021/acs.jpcb.3c00038
J. Phys. Chem. B 2023, 127, 2381−2394

for assaying LD phenotypes of obesity. By coupling SRS microscopy with Raman tags, Cheng et al. found that not only the newly uptake fatty acids but also cholesterol appeared mainly inside LDs in *C. elegans*.[49,72,73] Such LD accumulation in *C. elegans* opens new opportunities to study lipid metabolism in other animal models such as zebrafish and mice. By combining the hyperspectral SRS microscopy in the fingerprint region and quantitative multivariate curve resolution (MCR) analysis, Wang et al. demonstrated the quantitative mapping of lysosome-related organelles (LROs), LDs, oxidized lipids, and protein-rich organelles in distinct sites of intestinal cells in wild-type N2 *C. elegans* and *daf-2 (e1370)* mutants, which bear a mutation of insulin-like growth factor 1 (IGF-1) receptor[74] (Figure 3c). Compared to the wild-type, the *daf-2* insulin/IGF-1 receptor mutants show significantly increased LROs, LD storages, and oxidized lipids, suggesting that the insulin/IGF-1 signaling pathway regulates not only the LD storage but also lipid oxidation. With the capability of quantitative mapping of specific lipid species in LDs, SRS microscopy has been promised to give new insight into the impact of signaling pathway on obesity from *C. elegans* to mammals. Besides, the lipid metabolism exhibits significant intercellular variability, including the LD number, size, and composition. Lipid accumulation in nonadipocyte cells is mainly reflected in the increase of LD number, as opposed to an increase in LD size or average intensity of LDs during adipocyte differentiation.[75,76] As adipose tissue is the major organ for lipid storage, Zhu et al. explored the formation of LDs during adipogenesis and demonstrated that acyl-coenzyme A (CoA): cholesterol acyltransferases (ACATs) are required for storage of both TG and CE in adipocytes.[77] Taken together, SRS microscopy opens new opportunities to elucidate the essential role of LD in obesity.

Abnormal lipid metabolism plays a prominent role in atherosclerotic disease progression. Excessive CE storage in LDs of foam cells has been recognized as a hallmark of atherosclerotic cardiovascular diseases. By combining hyperspectral SRS microscopy with MCR analysis, Wang et al. developed a label-free quantitative imaging method of cholesterol storage in intact atherosclerotic arterial tissues based on the fingerprint Raman bands, indicating that cholesteryl oleate is the major component inside the lipid droplets of atherosclerotic arteries.[78] In particular, they employed the sterol C═C band at 1669 cm^{-1} as a characteristic band of cholesterol. Other significant Raman bands in the same spectral window, including the acyl C═C band, the ester C═O band, and the amide I band, were recorded simultaneously. By integrating hyperspectral SRS microscopy and second harmonic generation (SHG) microscopy on the same platform, Suhalim et al. discriminated cholesterol monohydrate crystals from condensed CEs in atherosclerotic plaques.[79] SHG is exclusively sensitive to noncentrosymmetric materials such as chiral crystals, and thus can be used to complement hyperspectral SRS in discriminating cholesterol crystals from other amorphous lipids, like CEs. However, the nonvanishing SHG activity of other structures in the tissue indicates that SHG microscopy alone is insufficient for identifying cholesterol crystal materials in atherosclerotic plaques, underlining the merits of a combined hyperspectral SRS and SHG approach. With alkyne tags, Wei et al. depicted the formation of numerous LDs that indicates transformation into foam cells (Figure 3d),[73] a hallmark of early atherosclerosis. To summarize, SRS microscopy opens new opportunities for identifying the atherosclerotic diseases through the study of CE accumulation in LDs.

The composition, spatial distribution, and temporal dynamics of LDs vary in different metabolic pathology. It was found that unsaturated fatty acid has preferential uptake into LD while saturated fatty acid exhibits toxicity in hepatic cells[26] (Figure 3e,f). The abnormal membrane-like structures were observed in saturated fatty acid labeled cells, while these structures were decreased by incorporation of unsaturated fatty acids. Those phenotypic changes in saturated fatty acids labeled cells may be due to alterations in membrane fluidity and/or structure as a result of increased saturation of membrane lipids, which is likely associated with the cytotoxicity of saturated fatty acids.

Taken together, SRS microscopy is a desirable approach to study LD biology in obesity and atherosclerosis, providing great potential in early diagnosis of disease, monitoring of therapy efficacy, and investigation of disease pathogenesis. Notably, many other metabolic diseases, e.g. fatty liver disease[80] and diabetes,[81] are also closely related to abnormal accumulation of LDs. In the future, we expect SRS microscopy can be used to decipher the processes of LD formation, budding, lipolysis, and secretion in liver pathologies and diabetes, which may ultimately lead to novel molecular therapies.

SRS Imaging of LDs in Cancer. Lipid metabolic reprogramming is critically involved in the development and progression of cancer.[82,83] As a reservoir for lipids, LD has been commonly seen in various cancers to store excessive newly synthesized lipids on one hand and provide lipids for hydrolysis and subsequent energy supply on the other hand. As early as the 1970s, LDs were observed in human breast cancer.[84] Since then, LD accumulation has been reported in many types of human cancers, including colon, brain, and others.[85,86] Nevertheless, the exact role of LD in cancer development and progression remains elusive.

In recent years, SRS microscopy has been used to study LD biology in human cancers. By integrating SRS microscopy with spontaneous Raman spectroscopy on the same platform, Yue et al. performed quantitative analysis of LD amount and composition at the single-cell level in intact human cancerous tissues. Enabled by such unique compositional analysis of LD *in situ*, the authors revealed an unexpected, aberrant accumulation of esterified cholesterol in LDs of high-grade prostate cancer and metastases[87] (Figure 4a,b). Further studies collectively revealed that cholesterol esterification could become a novel metabolic target for treating advanced prostate cancer.[88,89] Following these studies, elevated cholesterol esterification and CE accumulation have also been found in other types of aggressive human cancers, such as pancreatic cancer,[90] anaplastic large cell lymphoma,[91] and metastatic melanoma,[92] suggesting that CE in LD may be an universal metabolic vulnerability of human cancers.

Multicolor SRS microscopy has been used to readily detect many diagnostic signatures that are essential for brain tumor identification and classification. Through correlating large-scale SRS imaging with histopathology, Lu et al. revealed abundant intracellular LDs within the glioma cells, a feature that is not detectable by standard hematoxylin and eosin (H&E)-stained sections.[93] Subsequently, Bae et al. reported the biochemical variations and morphological differences between proneural and mesenchymal subtypes of glioblastomas (GBMs) by using

https://doi.org/10.1021/acs.jpcb.3c00038
J. Phys. Chem. B 2023, 127, 2381−2394

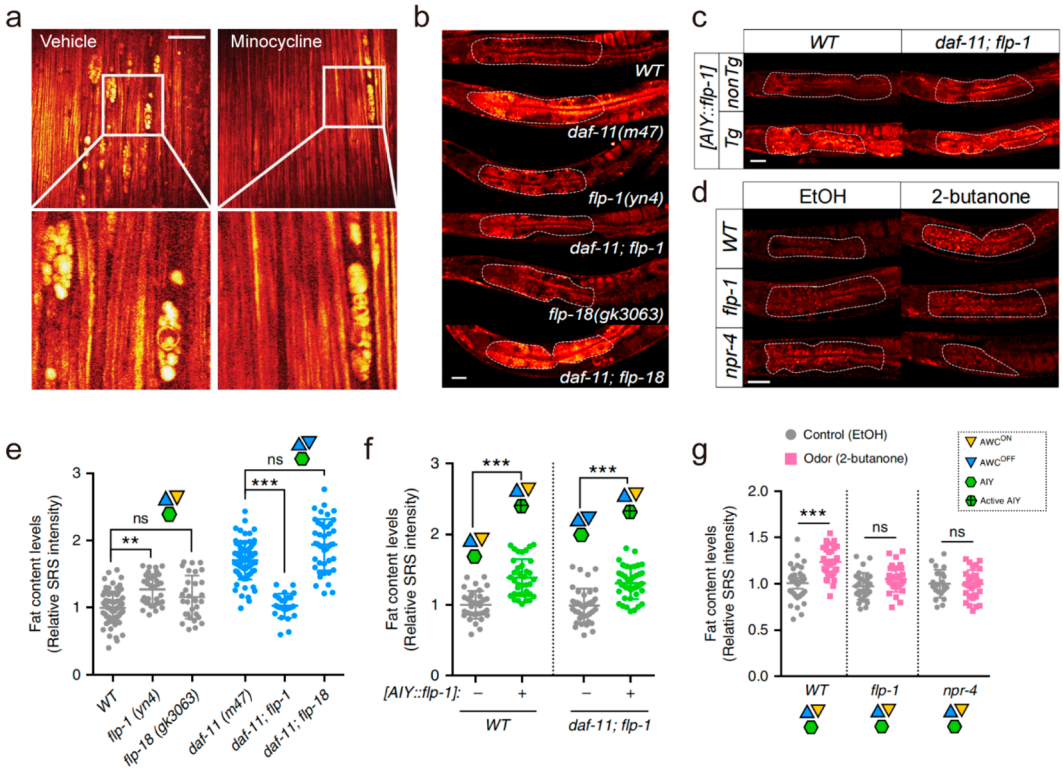

Figure 5. Stimulated Raman scattering (SRS) imaging of lipid droplets (LDs) in degenerative disorder. (a) SOD1G93A versus WT long-term serial *in vivo* SRS images at 8 weeks postnatal. Scale bar, 50 μm. (b–g) Neuropeptide signals link olfactory neural circuit and fat metabolism. (b, e) Among the neuropeptides that are secreted from AIY interneurons, deletion of flp-1, not flp-18, suppresses the increased fat storage in the daf-11 mutants. (c, f) AIY-specific overexpression of flp-1 increases fat storage under WT conditions. Restoration of flp-1 expression only in AIY neurons is sufficient to rescue fat storage increase in the daf-11; flp-1 double mutants. (d, g) Mutation of either flp-1 neuropeptide or its putative receptor npr-4 fully suppresses the fat storage increase conferred by the 2-butanone odor exposure. Scale bar, 40 μm. Panel a adapted with permission from ref 106 licensed under https://creativecommons.org/licenses/by/4.0/. Panels b–g adapted with permission from ref 108 licensed under https://creativecommons.org/licenses/by/4.0/.

hyperspectral SRS microscopy.[94] Compared to the abundance of cellular proteins in proneural GBMs, the mesenchymal GBM is characterized by LD accumulation.

Multiplex and hyperspectral SRS microscopy with advantages in complex compositional analysis has tremendously improved understanding of the role of LD in cancer progression. Liao et al. developed a new multiplex SRS microscope with a pixel dwell time down to tens of microseconds, which permits fast and quantitative analysis of LD composition, e.g., percentage of TG and CE in individual LDs (Figure 4c), in single live cancer cells.[39] Huang et al. subsequently developed a multiplex SRS imaging cytometry, which enabled acquisition of a Raman spectrum covering 200 wavenumbers at a speed of 5 μs in 32 spectral channels with a throughput of 30–50 cells per second.[95] Based on this technique, the authors distinguished 260 morphological and metabolic features in thousands of individual cells and unveiled that LDs actively transport from the cell body to protrusions, which might promote cancer cell survival under stress by enhancing their nutrient uptake capacity. Taking advantage of SRS imaging cytometry, LD-enriched protrusions were discovered to serve as a metabolic marker for cancer cells under stresses. By using hyperspectral SRS microscopy, Li et al. unraveled a significant increase of unsaturated lipids in LDs in ovarian cancer stem cells (CSCs) as compared to non-CSCs and demonstrated that lipid desaturation could be an effective metabolic target for ovarian therapy.[96] Interestingly, different from ovarian cancer, Yan et al. found a substantial amount of saturated lipid accumulation in LDs in human hepatocellular carcinoma tissues, but not in their adjacent normal tissues, suggesting that the aberrantly accumulated saturated lipids may have great potential to be a metabolic marker for human liver cancer.[97] More recently, by integrating hyperspectral SRS microscopy and transcriptomics analysis, Du et al. established a transcriptional relationship between cellular dedifferentiation and metabolic reprogramming among distinct BRAF mutant melanoma cancer cell phenotypes.[98] Then, the authors identified a previously unknown susceptibility of lipid monounsaturation within dedifferentiated mesenchymal cells with innate resistance to BRAF inhibition (Figure 4d), which validates the ability of SRS imaging to identify specific targeted metabolites.

Deuterated molecules have been used as Raman probes to study lipid metabolism in cancer. Both lipid synthesis via the *de novo* lipogenesis pathway and direct uptake of fatty acids can be stored in LDs. For example, SRS imaging has extensively demonstrated the incorporation of deuterated-glucose (glucose-d_7) and uptake of deuterated-fatty acids into LDs through either *de novo* lipogenesis or direct uptake. By coupling SRS microscopy with glucose-d_7, Li et al. revealed that lipids stored in LDs largely arose from *de novo* lipid synthesis in pancreatic cancer cells but not prostate cancer cells, which primarily relied on fatty acid uptake.[50] By using SRS microscopy to track deuterated-palmitate acid (PA-d_{31})/deuterated-oleate acid

https://doi.org/10.1021/acs.jpcb.3c00038
J. Phys. Chem. B 2023, 127, 2381–2394

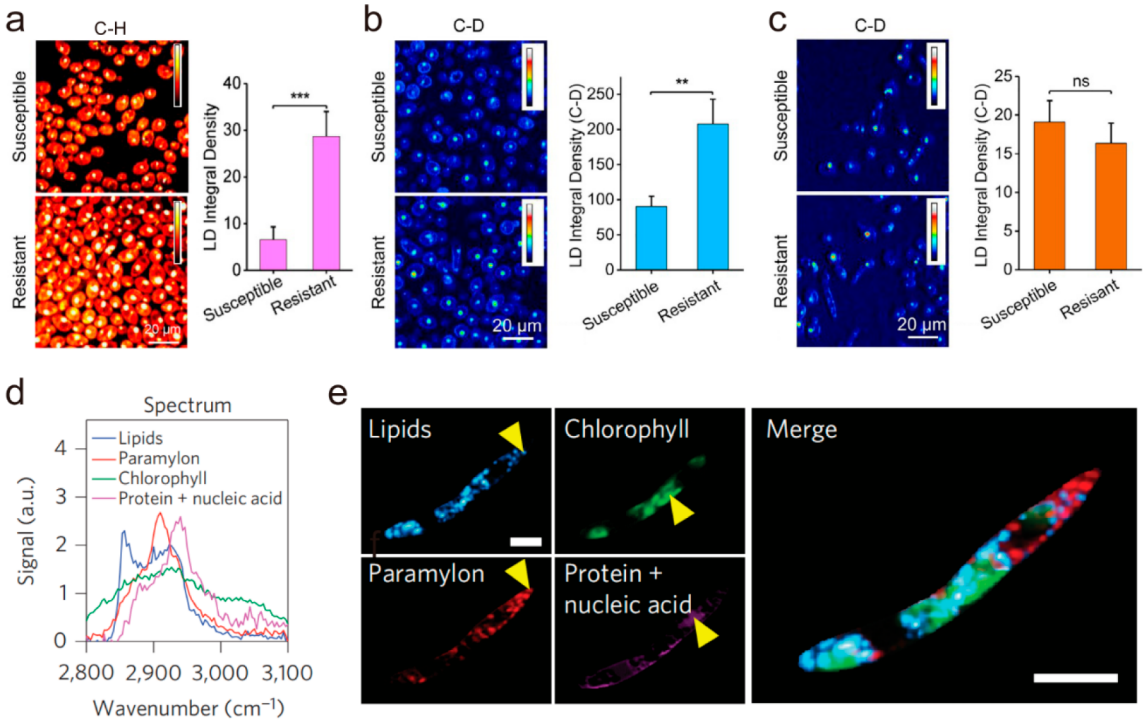

Figure 6. Stimulated Raman scattering (SRS) imaging of lipid droplets (LDs) in microbiology. (a) C−H frequency (2850 cm^{-1}) SRS images of fluconazole-susceptible and -resistant *C. albicans*. Quantification of lipid signal from both the fluconazole-susceptible and -resistant *C. albicans* strains. Student's *t* test was used for statistical analysis. (b) Visualization of *de novo* lipogenesis via C−D frequency (2120 cm^{-1}) SRS imaging. Quantification of LDs C−D signal shows that *de novo* lipogenesis is higher in the fluconazole-resistant strain. (c) Visualization of fatty acid uptake by fluconazole-susceptible and -resistant *C. albicans* strains via C−D frequency (2120 cm^{-1}) SRS imaging. Quantification of fatty acid uptake by fluconazole-susceptible and -resistant *C. albicans* strains. Twenty cells were analyzed for each strain. Student's *t* test was used for statistical analysis. ***$P < 0.001$; **$P < 0.01$; ns, not significant. (d, e) SRS imaging of fixed *E. gracilis* at 91 spectral points. The spectra of the chemical constituents were extracted from the points indicated by yellow arrows. Scale bar: 10 μm. Panels a−c adapted with permission from ref 113. Copyright 2017 American Chemical Society. Panels d and e adapted with permission from ref 31. Copyright 2016 Springer Nature.

(OA-d_{34}), Zhao et al. investigated how the dynamics between saturated fatty acids and unsaturated fatty acids regulated by stearoyl Co-A desaturase (SCD) impacted on ovarian cancer cell survival and tumor progression. The authors demonstrated that SCD was a key regulator of the cancer cell fate under metabolic stress and offered new treatment strategies by adjusting the lipid balance.[99] More recently, through high-throughput SRS imaging of glucose-d_7, PA-d_{31}, and OA-d_{34}, Tan et al. identified a stable metabolic switch from glucose and glycolysis dependent on fatty acid uptake and fatty acid β-oxidation dependent anabolic and energy metabolism in cisplatin-resistant ovarian cancer cells[100] (Figure 4e). In addition, blocking β-oxidation by a small molecule inhibitor suppresses ovarian cancer proliferation *in vitro* and growth of patient-derived xenografts *in vivo*, which provides promising treatment options for patients with cisplatin-resistant tumors by targeting the FAO pathway.

Taken together, SRS microscopy offers a novel platform to monitor dynamics of essential biomolecules and drug molecules in individual cancer cells and discover hidden signatures underlying LD accumulation, such as the cholesterol esterification, lipid desaturation, and lipid oxidation. Considering cell heterogeneity in a complex tumor microenvironment, it has become increasingly important to achieve quantitative, selective, and rapid screening of anticancer drug activity with an intact microenvironment at the subcellular level.[101] In the future, through more complex preclinical models, e.g. organoids and tissues, SRS microscopy is expected to elucidate the complex roles of LDs in modulation of anticancer drug sensitivity and discover more potential therapeutic targets for human cancers.

SRS Imaging of LDs in Neurodegenerative Disorder. Lipid metabolism plays a crucial role in maintenance of membrane functions and signaling events in the nervous system.[102] More recently, studies have identified the presence of LDs in neurons under certain disease conditions and demonstrated that disruption of LD function contributes to degenerative disorder.[103,104] Amyotrophic lateral sclerosis (ALS), a progressive neurodegenerative neuromuscular disease that progresses fast and is fatal, has also been found to be associated with abnormal LDs accumulation.[105] By SRS microscopy, Tian et al. revealed that lipid ovoid (ovoid structures with high lipid content) accumulation in the peripheral nerves of presymptomatic ALS animals were most likely lipids derived from degenerating myelinating cells.[106] The authors further demonstrated that SRS imaging could be employed to evaluate candidate therapeutics (Figure 5a), confirming that the compound minocycline significantly slows peripheral nerve degeneration in the *SOD1G93A* end-stage paralysis mouse. As a group of neurodegenerative disorders, polyglutamine (polyQ) diseases involve the deposition of aggregation-prone proteins with long polyQ expansions. By coupling SRS microscopy with deuterium-labeled glutamine, Miao et al. achieved imaging of native polyQ aggregates without the need of large fusion proteins and developed a ratiometric strategy for quantitative analysis of different

https://doi.org/10.1021/acs.jpcb.3c00038
J. Phys. Chem. B 2023, 127, 2381−2394

structures in aggregates of varying sizes, including nucleoli and LDs,[107] which could help unequivocally differentiate aggregates from other puncta-like structures. More recently, Mutlu et al. discovered that 2-butanone and its responding olfactory neuron act through a selective neural circuit and downstream neuroendocrine pathway to directly regulate peripheral fat metabolism without affecting eating behaviors (Figure 5b−g), supporting the high selectivity of the olfactory sense in fine-tuning metabolic physiology.[108] Collectively, SRS microscopy is a sensitive and quantitative means of measuring LD alteration during neurodegenerative disorders. Notably, there are more neurodegenerative diseases related to LD dysregulation, such as Alzheimer's disease[109] and Parkinson's disease.[104] In the future, SRS microscopy is expected to extend the study of LD biology to a wider range of degenerative diseases, which may provide new therapeutic strategies.

SRS Imaging of LDs in Microbiology. Antimicrobial resistance threatens the effective treatment of infectious diseases caused by bacteria and fungi. Rapid antimicrobial susceptibility testing (AST) plays a major role in suppressing the emergence of antimicrobial resistance and consequently reduces the deaths caused by drug-resistant infections. Due to the high imaging speed capability, SRS microscopy incorporated with glucose-d_7[110] or D_2O has been used for the rapid determination of antimicrobial susceptibility.[111,112] Beyond SRS-based AST, Karanja et al. used SRS imaging to reveal aberrant LD accumulation in fluconazole-resistant but not fluconazole-susceptible *C. albicans*[113] (Figure 6a−c), opening a new way to detect and treat resistant fungal infections. Using multicolor SRS microscopy, a recent work reported by Wakisaka et al. demonstrated the intracellular metabolite distributions of paramylon, lipids, and chlorophyll[31] under different culture conditions in live *E. gracilis* (Figure 6d,e), providing insights into understanding microalgal heterogeneity, optimizing culture methods, and screening mutant microalgae. Taken together, SRS microscopy not only is a feasible platform for rapid detection of antimicrobial susceptibility by direct imaging of LD activity, but also provides further insights into microbial heterogeneity. Due to the wide variety of microorganisms and severe drug resistance problems, SRS microscopy is expected to focus more on the role of LD in microbiology, which may lead to novel AST methods and antimicrobial agents.

CONCLUSION

As a critical hub of intracellular lipid metabolism, LD maintains dynamic homeostasis, and its dysregulation may promote pathogenetic mechanisms. Deeper understanding of LD biology, such as biogenesis, mobility, and heterogeneity, will provide new opportunities for therapeutic intervention. Owing to the capability of high detection sensitivity, high molecular specificity, and high spatiotemporal resolution, SRS microscopy has become a versatile and robust characterization platform for the study of the distribution, composition, and dynamics of LDs in a wide range of living biological species. Development of hyperspectral and multiplex SRS microscopy enables extraction of quantitative concentration maps of specific lipid species in complex biological systems. Incorporation of Raman tags makes SRS microscopy further gain superb chemical selectivity and sensitivity to pinpoint molecules of interest in complex living systems, which offers the possibility of yielding new understanding for LD biology.

Moreover, we believe technical advancements in SRS microscopy would further promote the research field of LD biology. First, super resolution SRS microscopy, e.g. near-resonance enhanced label-free SRS microscopy approaching 130 nm,[114] may allow direct visualization of small-sized LDs and the whole dynamic process of LD biogenesis, which is fundamental for the understanding of LD biology. Second, ultrafast SRS microscopy, e.g. video-rate SRS microscopy at 100 ns/pixel[115] and SRS microscope based on collinear multiple beams (COMB-SRS) at 2000 frames/s,[116] may permit monitoring of LD trafficking and interaction of LD with other organelles (endoplasmic reticulum, mitochondria, etc.) three-dimensionally in living organisms during development. Third, novel hyperspectral image analysis methods[74,95,117,118] can be incorporated to existing spectral unmixing frameworks to further improve its performance in several aspects, including higher sensitivity to unknown species and better distinguishability to specific components. It is also expected that deep learning-based classification will further improve performance such as higher accuracy, less training sample size, and faster training time for identification of more LD biomarkers in various diseases. Fourth, the SRS imaging flow cytometry[95,119] and sorting[120] are expected to provide high-throughput and high-content information regarding LD at the single cell level, which may be useful for label-free sorting of well-differentiated adipocytes, cell/microbe subtyping, and *in vitro* diagnostics. Looking into the future, SRS microscopy will further improve our understanding of LD biology and promote a wider range of life science and medical translations.

AUTHOR INFORMATION

Corresponding Author

Shuhua Yue − *Key Laboratory of Biomechanics and Mechanobiology (Beihang University), Ministry of Education, Institute of Medical Photonics, Beijing Advanced Innovation Center for Biomedical Engineering, School of Biological Science and Medical Engineering, Beihang University, Beijing 100191, China;* orcid.org/0000-0003-1830-008X; Email: yue_shuhua@buaa.edu.cn

Author

Hao Jia − *Key Laboratory of Biomechanics and Mechanobiology (Beihang University), Ministry of Education, Institute of Medical Photonics, Beijing Advanced Innovation Center for Biomedical Engineering, School of Biological Science and Medical Engineering, Beihang University, Beijing 100191, China;* orcid.org/0000-0003-0146-6171

Complete contact information is available at: https://pubs.acs.org/10.1021/acs.jpcb.3c00038

Author Contributions

H.J. contributed to the systematic review of the literature and wrote the initial draft of the manuscript. S.Y. wrote the review article and critically analyzed and approved it.

Notes

The authors declare no competing financial interest.

ACKNOWLEDGMENTS

This work is supported by National Natural Science Foundation of China (No. 62027824, No. 91959120) and

Fundamental Research Funds for the Central Universities (No. YWF-22-L-547).

REFERENCES

(1) Thiam, A. R.; Ikonen, E. Lipid Droplet Nucleation. *Trends Cell Biol.* **2021**, *31* (2), 108−118.

(2) Walther, T. C.; Farese, R. V., Jr. Lipid droplets and cellular lipid metabolism. *Annu. Rev. Biochem.* **2012**, *81*, 687−714.

(3) Olzmann, J. A.; Carvalho, P. Dynamics and functions of lipid droplets. *Nat. Rev. Mol. Cell Biol.* **2019**, *20* (3), 137−155.

(4) Rinia, H. A.; Burger, K. N.; Bonn, M.; Muller, M. Quantitative label-free imaging of lipid composition and packing of individual cellular lipid droplets using multiplex CARS microscopy. *Biophys. J.* **2008**, *95* (10), 4908−4914.

(5) Hsieh, K.; Lee, Y. K.; Londos, C.; Raaka, B. M.; Dalen, K. T.; Kimmel, A. R. Perilipin family members preferentially sequester to either triacylglycerol-specific or cholesteryl-ester-specific intracellular lipid storage droplets. *J. Cell Sci.* **2012**, *125* (17), 4067−4076.

(6) Buchberger, A. R.; DeLaney, K.; Johnson, J.; Li, L. Mass Spectrometry Imaging: A Review of Emerging Advancements and Future Insights. *Anal. Chem.* **2018**, *90* (1), 240−265.

(7) Hall, Z.; Chiarugi, D.; Charidemou, E.; Leslie, J.; Scott, E.; Pellegrinet, L.; Allison, M.; Mocciaro, G.; Anstee, Q. M.; Evan, G. I.; et al. Lipid Remodeling in Hepatocyte Proliferation and Hepatocellular Carcinoma. *Hepatology* **2021**, *73* (3), 1028−1044.

(8) Slipchenko, M. N.; Le, T. T.; Chen, H.; Cheng, J. X. High-speed vibrational imaging and spectral analysis of lipid bodies by compound Raman microscopy. *J. Phys. Chem. B* **2009**, *113* (21), 7681−7686.

(9) Jones, R. R.; Hooper, D. C.; Zhang, L.; Wolverson, D.; Valev, V. K. Raman Techniques: Fundamentals and Frontiers. *Nanoscale Res. Lett.* **2019**, *14* (1), 231.

(10) De Gelder, J.; De Gussem, K.; Vandenabeele, P.; Moens, L. Reference database of Raman spectra of biological molecules. *J. Raman Spectrosc.* **2007**, *38* (9), 1133−1147.

(11) Vidavsky, N.; Kunitake, J.; Diaz-Rubio, M. E.; Chiou, A. E.; Loh, H. C.; Zhang, S.; Masic, A.; Fischbach, C.; Estroff, L. A. Mapping and Profiling Lipid Distribution in a 3D Model of Breast Cancer Progression. *ACS Cent Sci.* **2019**, *5* (5), 768−780.

(12) Allakhverdiev, E. S.; Khabatova, V. V.; Kossalbayev, B. D.; Zadneprovskaya, E. V.; Rodnenkov, O. V.; Martynyuk, T. V.; Maksimov, G. V.; Alwasel, S.; Tomo, T.; Allakhverdiev, S. I. Raman Spectroscopy and Its Modifications Applied to Biological and Medical Research. *Cells* **2022**, *11* (3), 386.

(13) Cheng, J.-X.; Xie, X. S. *Coherent Raman Scattering Microscopy*; CRC Press, 2012.

(14) Liao, C. S.; Cheng, J. X. In Situ and In Vivo Molecular Analysis by Coherent Raman Scattering Microscopy. *Annu. Rev. Anal Chem. (Palo Alto Calif)* **2016**, *9* (1), 69−93.

(15) Yue, S.; Cheng, J. X. Deciphering single cell metabolism by coherent Raman scattering microscopy. *Curr. Opin Chem. Biol.* **2016**, *33*, 46−57.

(16) Cheng, J. X.; Xie, X. S. Vibrational spectroscopic imaging of living systems: An emerging platform for biology and medicine. *Science* **2015**, *350* (6264), aaa8870.

(17) Chen, W. W.; Lemieux, G. A.; Camp, C. H., Jr.; Chang, T. C.; Ashrafi, K.; Cicerone, M. T. Spectroscopic coherent Raman imaging of Caenorhabditis elegans reveals lipid particle diversity. *Nat. Chem. Biol.* **2020**, *16* (10), 1087−1095.

(18) Nan, X.; Cheng, J. X.; Xie, X. S. Vibrational imaging of lipid droplets in live fibroblast cells with coherent anti-Stokes Raman scattering microscopy. *J. Lipid Res.* **2003**, *44* (11), 2202−2208.

(19) Le, T. T.; Cheng, J. X. Single-cell profiling reveals the origin of phenotypic variability in adipogenesis. *PLoS One* **2009**, *4* (4), No. e5189.

(20) Le, T. T.; Yue, S.; Cheng, J. X. Shedding new light on lipid biology with coherent anti-Stokes Raman scattering microscopy. *J. Lipid Res.* **2010**, *51* (11), 3091−3102.

(21) Freudiger, C. W.; Min, W.; Saar, B. G.; Lu, S.; Holtom, G. R.; He, C.; Tsai, J. C.; Kang, J. X.; Xie, X. S. Label-free biomedical imaging with high sensitivity by stimulated Raman scattering microscopy. *Science* **2008**, *322* (5909), 1857−1861.

(22) Chen, T.; Yavuz, A.; Wang, M. C. Dissecting lipid droplet biology with coherent Raman scattering microscopy. *J. Cell Sci.* **2022**, *135* (5), jcs252353.

(23) Zhang, C.; Zhang, D.; Cheng, J. X. Coherent Raman Scattering Microscopy in Biology and Medicine. *Annu. Rev. Biomed Eng.* **2015**, *17*, 415−445.

(24) Fung, A. A.; Shi, L. Mammalian cell and tissue imaging using Raman and coherent Raman microscopy. *WIREs Mechanisms of Disease* **2020**, *12* (6), No. e1501.

(25) Cheng, K.-X.; Min, W.; Ozeki, Y.; Polli, D. *Stimulated Raman Scattering Microscopy Techniques and Applications*; Elsevier, 2021.

(26) Fu, D.; Yu, Y.; Folick, A.; Currie, E.; Farese, R. V., Jr.; Tsai, T. H.; Xie, X. S.; Wang, M. C. In vivo metabolic fingerprinting of neutral lipids with hyperspectral stimulated Raman scattering microscopy. *J. Am. Chem. Soc.* **2014**, *136* (24), 8820−8828.

(27) Hong, S.; Chen, T.; Liu, L.; Cao, C.; Lv, F.; Rabinowitz, J. D.; Huang, Y.; Chen, X. Live-Cell Imaging of NADPH Production from Specific Pathways. *CCS Chemistry* **2021**, *3* (6), 1642−1648.

(28) Li, X.; Li, Y.; Jiang, M.; Wu, W.; He, S.; Chen, C.; Qin, Z.; Tang, B. Z.; Mak, H. Y.; Qu, J. Y. Quantitative Imaging of Lipid Synthesis and Lipolysis Dynamics in Caenorhabditis elegans by Stimulated Raman Scattering Microscopy. *Anal. Chem.* **2019**, *91* (3), 2279−2287.

(29) Adams, W. R.; Gautam, R.; Locke, A.; Masson, L. E.; Borrachero-Conejo, A. I.; Dollinger, B. R.; Throckmorton, G. A.; Duvall, C.; Jansen, E. D.; Mahadevan-Jansen, A. Visualizing the lipid dynamics role in infrared neural stimulation using stimulated Raman scattering. *Biophys. J.* **2022**, *121* (8), 1525−1540.

(30) Lu, F. K.; Ji, M.; Fu, D.; Ni, X.; Freudiger, C. W.; Holtom, G.; Xie, X. S. Multicolor stimulated Raman scattering (SRS) microscopy. *Mol. Phys.* **2012**, *110* (15−16), 1927−1932.

(31) Wakisaka, Y.; Suzuki, Y.; Iwata, O.; Nakashima, A.; Ito, T.; Hirose, M.; Domon, R.; Sugawara, M.; Tsumura, N.; Watarai, H.; et al. Probing the metabolic heterogeneity of live Euglena gracilis with stimulated Raman scattering microscopy. *Nat. Microbiol* **2016**, *1* (10), 16124.

(32) Satoh, S.; Otsuka, Y.; Ozeki, Y.; Itoh, K.; Hashiguchi, A.; Yamazaki, K.; Hashimoto, H.; Sakamoto, M. Label-free visualization of acetaminophen-induced liver injury by high-speed stimulated Raman scattering spectral microscopy and multivariate image analysis. *Pathol Int.* **2014**, *64* (10), 518−526.

(33) Shi, L.; Zheng, C.; Shen, Y.; Chen, Z.; Silveira, E. S.; Zhang, L.; Wei, M.; Liu, C.; de Sena-Tomas, C.; Targoff, K.; et al. Optical imaging of metabolic dynamics in animals. *Nat. Commun.* **2018**, *9* (1), 2995.

(34) Zhang, L.; Shi, L.; Shen, Y.; Miao, Y.; Wei, M.; Qian, N.; Liu, Y.; Min, W. Spectral tracing of deuterium for imaging glucose metabolism. *Nat. Biomed Eng.* **2019**, *3* (5), 402−413.

(35) Oh, S.; Lee, C.; Yang, W.; Li, A.; Mukherjee, A.; Basan, M.; Ran, C.; Yin, W.; Tabin, C. J.; Fu, D.; et al. Protein and lipid mass concentration measurement in tissues by stimulated Raman scattering microscopy. *Proc. Natl. Acad. Sci. U. S. A.* **2022**, *119* (17), No. e2117938119.

(36) Camp Jr, C. H.; Lee, Y. J.; Heddleston, J. M.; Hartshorn, C. M.; Walker, A. R. H.; Rich, J. N.; Lathia, J. D.; Cicerone, M. T. High-Speed Coherent Raman Fingerprint Imaging of Biological Tissues. *Nat. Photonics* **2014**, *8*, 627−634.

(37) Réhault, J.; Crisafi, F.; Kumar, V.; Ciardi, G.; Marangoni, M.; Cerullo, G.; Polli, D. Broadband stimulated Raman scattering with Fourier-transform detection. *Opt Express* **2015**, *23* (19), 25235−25246.

(38) Fu, D.; Lu, F. K.; Zhang, X.; Freudiger, C.; Pernik, D. R.; Holtom, G.; Xie, X. S. Quantitative chemical imaging with multiplex stimulated Raman scattering microscopy. *J. Am. Chem. Soc.* **2012**, *134* (8), 3623−3626.

(39) Liao, C. S.; Slipchenko, M. N.; Wang, P.; Li, J.; Lee, S. Y.; Oglesbee, R. A.; Cheng, J. X. Microsecond Scale Vibrational

https://doi.org/10.1021/acs.jpcb.3c00038
J. Phys. Chem. B 2023, 127, 2381−2394

Spectroscopic Imaging by Multiplex Stimulated Raman Scattering Microscopy. *Light Sci. Appl.* **2015**, *4*, e265.
(40) Fu, D.; Holtom, G.; Freudiger, C.; Zhang, X.; Xie, X. S. Hyperspectral imaging with stimulated Raman scattering by chirped femtosecond lasers. *J. Phys. Chem. B* **2013**, *117* (16), 4634−4640.
(41) Liao, C.-S.; Huang, K.-C.; Hong, W.; Chen, A. J.; Karanja, C.; Wang, P.; Eakins, G.; Cheng, J.-X. Stimulated Raman spectroscopic imaging by microsecond delay-line tuning. *Optica* **2016**, *3* (12), 1377.
(42) He, R.; Liu, Z.; Xu, Y.; Huang, W.; Ma, H.; Ji, M. Stimulated Raman scattering microscopy and spectroscopy with a rapid scanning optical delay line. *Optics letters* **2017**, *42* (4), 659−662.
(43) Long, R.; Zhang, L.; Shi, L.; Shen, Y.; Hu, F.; Zeng, C.; Min, W. Two-color vibrational imaging of glucose metabolism using stimulated Raman scattering. *Chem. Commun.* **2018**, *54* (2), 152−155.
(44) Hu, F.; Zeng, C.; Long, R.; Miao, Y.; Wei, L.; Xu, Q.; Min, W. Supermultiplexed optical imaging and barcoding with engineered polyynes. *Nat. Methods* **2018**, *15* (3), 194−200.
(45) Shi, L.; Wei, M.; Miao, Y.; Qian, N.; Shi, L.; Singer, R. A.; Benninger, R. K. P.; Min, W. Highly-multiplexed volumetric mapping with Raman dye imaging and tissue clearing. *Nat. Biotechnol.* **2022**, *40* (3), 364−373.
(46) Wei, L.; Chen, Z.; Shi, L.; Long, R.; Anzalone, A. V.; Zhang, L.; Hu, F.; Yuste, R.; Cornish, V. W.; Min, W. Super-multiplex vibrational imaging. *Nature* **2017**, *544* (7651), 465−470.
(47) Shen, Y.; Hu, F.; Min, W. Raman Imaging of Small Biomolecules. *Annu. Rev. Biophys* **2019**, *48*, 347−369.
(48) Zhao, Z.; Shen, Y.; Hu, F.; Min, W. Applications of vibrational tags in biological imaging by Raman microscopy. *Analyst* **2017**, *142* (21), 4018−4029.
(49) Lee, H. J.; Zhang, W.; Zhang, D.; Yang, Y.; Liu, B.; Barker, E. L.; Buhman, K. K.; Slipchenko, L. V.; Dai, M.; Cheng, J. X. Assessing cholesterol storage in live cells and C. elegans by stimulated Raman scattering imaging of phenyl-Diyne cholesterol. *Sci. Rep* **2015**, *5*, 7930.
(50) Li, J.; Cheng, J. X. Direct visualization of de novo lipogenesis in single living cells. *Sci. Rep* **2014**, *4*, 6807.
(51) Shen, Y.; Zhao, Z.; Zhang, L.; Shi, L.; Shahriar, S.; Chan, R. B.; Di Paolo, G.; Min, W. Metabolic activity induces membrane phase separation in endoplasmic reticulum. *Proc. Natl. Acad. Sci. U. S. A.* **2017**, *114* (51), 13394−13399.
(52) Aizawa, R.; Ibayashi, M.; Tatsumi, T.; Yamamoto, A.; Kokubo, T.; Miyasaka, N.; Sato, K.; Ikeda, S.; Minami, N.; Tsukamoto, S. Synthesis and maintenance of lipid droplets are essential for mouse preimplantation embryonic development. *Development (Cambridge, England)* **2019**, *146* (22), dev.181925.
(53) Mau, K. H. T.; Karimlou, D.; Barneda, D.; Brochard, V.; Royer, C.; Leeke, B.; de Souza, R. A.; Pailles, M.; Percharde, M.; Srinivas, S.; et al. Dynamic enlargement and mobilization of lipid droplets in pluripotent cells coordinate morphogenesis during mouse peri-implantation development. *Nat. Commun.* **2022**, *13* (1), 3861.
(54) Ye, Q.; Zeng, X.; Cai, S.; Qiao, S.; Zeng, X. Mechanisms of lipid metabolism in uterine receptivity and embryo development. *Trends Endocrinol Metab* **2021**, *32* (12), 1015−1030.
(55) Watanabe, T.; Thayil, A.; Jesacher, A.; Grieve, K.; Debarre, D.; Wilson, T.; Booth, M.; Srinivas, S. Characterisation of the dynamic behaviour of lipid droplets in the early mouse embryo using adaptive harmonic generation microscopy. *BMC cell biology* **2010**, *11*, 38.
(56) Bradley, J.; Pope, I.; Masia, F.; Sanusi, R.; Langbein, W.; Swann, K.; Borri, P. Quantitative imaging of lipids in live mouse oocytes and early embryos using CARS microscopy. *Development (Cambridge, England)* **2016**, *143* (12), 2238−2247.
(57) Dou, W.; Zhang, D.; Jung, Y.; Cheng, J. X.; Umulis, D. M. Label-free imaging of lipid-droplet intracellular motion in early Drosophila embryos using femtosecond-stimulated Raman loss microscopy. *Biophys. J.* **2012**, *102* (7), 1666−1675.
(58) Han, M.; Chang, H.; Zhang, P.; Chen, T.; Zhao, Y.; Zhang, Y.; Liu, P.; Xu, T.; Xu, P. C13C4.5/Spinster, an evolutionarily conserved protein that regulates fertility in C. elegans through a lysosome-mediated lipid metabolism process. *Protein Cell* **2013**, *4* (5), 364−372.
(59) Chen, A. J.; Li, J.; Jannasch, A.; Mutlu, A. S.; Wang, M. C.; Cheng, J. X. Fingerprint Stimulated Raman Scattering Imaging Reveals Retinoid Coupling Lipid Metabolism and Survival. *ChemPhysChem* **2018**, *19* (19), 2500−2506.
(60) Johnson, A. A.; Stolzing, A. The role of lipid metabolism in aging, lifespan regulation, and age-related disease. *Aging Cell* **2019**, *18* (6), No. e13048.
(61) Beas, A. O.; Gordon, P. B.; Prentiss, C. L.; Olsen, C. P.; Kukurugya, M. A.; Bennett, B. D.; Parkhurst, S. M.; Gottschling, D. E. Independent regulation of age associated fat accumulation and longevity. *Nat. Commun.* **2020**, *11* (1), 2790.
(62) Mutlu, A. S.; Duffy, J.; Wang, M. C. Lipid metabolism and lipid signals in aging and longevity. *Dev Cell* **2021**, *56* (10), 1394−1407.
(63) Ratnappan, R.; Amrit, F. R.; Chen, S. W.; Gill, H.; Holden, K.; Ward, J.; Yamamoto, K. R.; Olsen, C. P.; Ghazi, A. Germline signals deploy NHR-49 to modulate fatty-acid β-oxidation and desaturation in somatic tissues of C. elegans. *PLoS genetics* **2014**, *10* (12), No. e1004829.
(64) Ramachandran, P. V.; Savini, M.; Folick, A. K.; Hu, K.; Masand, R.; Graham, B. H.; Wang, M. C. Lysosomal Signaling Promotes Longevity by Adjusting Mitochondrial Activity. *Dev Cell* **2019**, *48* (5), 685−696.
(65) Li, Y.; Zhang, W.; Fung, A. A.; Shi, L. DO-SRS imaging of metabolic dynamics in aging Drosophila. *Analyst* **2021**, *146* (24), 7510−7519.
(66) Li, Y.; Zhang, W.; Fung, A. A.; Shi, L. DO-SRS imaging of diet regulated metabolic activities in Drosophila during aging processes. *Aging Cell* **2022**, *21* (4), No. e13586.
(67) Greenberg, A. S.; Coleman, R. A.; Kraemer, F. B.; McManaman, J. L.; Obin, M. S.; Puri, V.; Yan, Q. W.; Miyoshi, H.; Mashek, D. G. The role of lipid droplets in metabolic disease in rodents and humans. *J. Clin Invest* **2011**, *121* (6), 2102−2110.
(68) Herker, E.; Vieyres, G.; Beller, M.; Krahmer, N.; Bohnert, M. Lipid Droplet Contact Sites in Health and Disease. *Trends Cell Biol.* **2021**, *31* (5), 345−358.
(69) Shen, P.; Yue, Y.; Zheng, J.; Park, Y. Caenorhabditis elegans: A Convenient In Vivo Model for Assessing the Impact of Food Bioactive Compounds on Obesity, Aging, and Alzheimer's Disease. *Annu. Rev. Food Sci. Technol.* **2018**, *9*, 1−22.
(70) Srinivasan, S. Regulation of body fat in Caenorhabditis elegans. *Annu. Rev. Physiol.* **2015**, *77*, 161−178.
(71) Wang, M. C.; Min, W.; Freudiger, C. W.; Ruvkun, G.; Xie, X. S. RNAi screening for fat regulatory genes with SRS microscopy. *Nat. Methods* **2011**, *8* (2), 135−138.
(72) Zhang, D.; Slipchenko, M. N.; Cheng, J. X. Highly Sensitive Vibrational Imaging by Femtosecond Pulse Stimulated Raman Loss. *J. Phys. Chem. Lett.* **2011**, *2* (11), 1248−1253.
(73) Wei, L.; Hu, F.; Shen, Y.; Chen, Z.; Yu, Y.; Lin, C. C.; Wang, M. C.; Min, W. Live-cell imaging of alkyne-tagged small biomolecules by stimulated Raman scattering. *Nat. Methods* **2014**, *11* (4), 410−412.
(74) Wang, P.; Liu, B.; Zhang, D.; Belew, M. Y.; Tissenbaum, H. A.; Cheng, J. X. Imaging lipid metabolism in live Caenorhabditis elegans using fingerprint vibrations. *Angew. Chem., Int. Ed. Engl.* **2014**, *53* (44), 11787−11792.
(75) Ferrara, M. A.; Filograna, A.; Ranjan, R.; Corda, D.; Valente, C.; Sirleto, L. Three-dimensional label-free imaging throughout adipocyte differentiation by stimulated Raman microscopy. *PLoS One* **2019**, *14* (5), No. e0216811.
(76) Cao, C.; Zhou, D.; Chen, T.; Streets, A. M.; Huang, Y. Label-Free Digital Quantification of Lipid Droplets in Single Cells by Stimulated Raman Microscopy on a Microfluidic Platform. *Anal. Chem.* **2016**, *88* (9), 4931−4939.
(77) Zhu, Y.; Chen, C. Y.; Li, J.; Cheng, J. X.; Jang, M.; Kim, K. H. In vitro exploration of ACAT contributions to lipid droplet formation during adipogenesis. *J. Lipid Res.* **2018**, *59* (5), 820−829.
(78) Wang, P.; Li, J.; Wang, P.; Hu, C. R.; Zhang, D.; Sturek, M.; Cheng, J. X. Label-free quantitative imaging of cholesterol in intact tissues by hyperspectral stimulated Raman scattering microscopy. *Angew. Chem., Int. Ed. Engl.* **2013**, *52* (49), 13042−13046.

https://doi.org/10.1021/acs.jpcb.3c00038
J. Phys. Chem. B 2023, 127, 2381−2394

(79) Suhalim, J. L.; Chung, C.-Y.; Lilledahl, M. B.; Lim, R. S.; Levi, M.; Tromberg, B. J.; Potma, E. O. Characterization of Cholesterol Crystals in Atherosclerotic Plaques Using Stimulated Raman Scattering and Second-Harmonic Generation Microscopy. *Biophys. J.* **2012**, *102* (8), 1988−1995.
(80) Gluchowski, N. L.; Becuwe, M.; Walther, T. C.; Farese, R. V. Jr. Lipid droplets and liver disease: from basic biology to clinical implications. *Nat. Rev. Gastroenterol Hepatol* **2017**, *14* (6), 343−355.
(81) Athyros, V. G.; Doumas, M.; Imprialos, K. P.; Stavropoulos, K.; Georgianou, E.; Katsimardou, A.; Karagiannis, A. Diabetes and lipid metabolism. *Hormones (Athens, Greece)* **2018**, *17* (1), 61−67.
(82) Menendez, J. A.; Lupu, R. Fatty acid synthase and the lipogenic phenotype in cancer pathogenesis. *Nat. Rev. Cancer* **2007**, *7* (10), 763−777.
(83) Currie, E.; Schulze, A.; Zechner, R.; Walther, T. C.; Farese, R. V., Jr. Cellular fatty acid metabolism and cancer. *Cell Metab* **2013**, *18* (2), 153−161.
(84) Ramos, C. V.; Taylor, H. B. Lipid-rich carcinoma of the breast. A clinicopathologic analysis of 13 examples. *Cancer* **1974**, *33* (3), 812−819.
(85) Accioly, M. T.; Pacheco, P.; Maya-Monteiro, C. M.; Carrossini, N.; Robbs, B. K.; Oliveira, S. S.; Kaufmann, C.; Morgado-Diaz, J. A.; Bozza, P. T.; Viola, J. P. Lipid bodies are reservoirs of cyclooxygenase-2 and sites of prostaglandin-E2 synthesis in colon cancer cells. *Cancer Res.* **2008**, *68* (6), 1732−1740.
(86) Jiang, Y.; Sun, A.; Zhao, Y.; Ying, W.; Sun, H.; Yang, X.; Xing, B.; Sun, W.; Ren, L.; Hu, B.; et al. Proteomics identifies new therapeutic targets of early-stage hepatocellular carcinoma. *Nature* **2019**, *567* (7747), 257−261.
(87) Yue, S.; Li, J.; Lee, S. Y.; Lee, H. J.; Shao, T.; Song, B.; Cheng, L.; Masterson, T. A.; Liu, X.; Ratliff, T. L.; et al. Cholesteryl ester accumulation induced by PTEN loss and PI3K/AKT activation underlies human prostate cancer aggressiveness. *Cell Metab* **2014**, *19* (3), 393−406.
(88) Lee, H. J.; Li, J.; Vickman, R. E.; Li, J.; Liu, R.; Durkes, A. C.; Elzey, B. D.; Yue, S.; Liu, X.; Ratliff, T. L.; et al. Cholesterol Esterification Inhibition Suppresses Prostate Cancer Metastasis by Impairing the Wnt/beta-catenin Pathway. *Mol. Cancer Res.* **2018**, *16* (6), 974−985.
(89) Chen, X.; Cui, S.; Yan, S.; Zhang, S.; Fan, Y.; Gong, Y.; Zhou, L.; Wang, P.; Yao, L.; Yue, S. Hyperspectral stimulated Raman scattering microscopy facilitates differentiation of low-grade and high-grade human prostate cancer. *J. Phys. D Appl. Phys.* **2021**, *54* (48), 484001.
(90) Li, J.; Gu, D.; Lee, S. S.; Song, B.; Bandyopadhyay, S.; Chen, S.; Konieczny, S. F.; Ratliff, T. L.; Liu, X.; Xie, J.; et al. Abrogating cholesterol esterification suppresses growth and metastasis of pancreatic cancer. *Oncogene* **2016**, *35* (50), 6378−6388.
(91) Garcia-Bermudez, J.; Baudrier, L.; Bayraktar, E. C.; Shen, Y.; La, K.; Guarecuco, R.; Yucel, B.; Fiore, D.; Tavora, B.; Freinkman, E.; et al. Squalene accumulation in cholesterol auxotrophic lymphomas prevents oxidative cell death. *Nature* **2019**, *567* (7746), 118−122.
(92) Lee, H. J.; Chen, Z.; Collard, M.; Chen, F.; Chen, J. G.; Wu, M.; Alani, R. M.; Cheng, J.-X. Multimodal Metabolic Imaging Reveals Pigment Reduction and Lipid Accumulation in Metastatic Melanoma. *BME Frontiers* **2021**, *2021*, 9860123.
(93) Lu, F. K.; Calligaris, D.; Olubiyi, O. I.; Norton, I.; Yang, W.; Santagata, S.; Xie, X. S.; Golby, A. J.; Agar, N. Y. Label-Free Neurosurgical Pathology with Stimulated Raman Imaging. *Cancer Res.* **2016**, *76* (12), 3451−3462.
(94) Bae, K.; Zheng, W.; Lin, K.; Lim, S. W.; Chong, Y. K.; Tang, C.; King, N. K.; Ti Ang, C. B.; Huang, Z. Epi-Detected Hyperspectral Stimulated Raman Scattering Microscopy for Label-Free Molecular Subtyping of Glioblastomas. *Anal. Chem.* **2018**, *90* (17), 10249−10255.
(95) Huang, K. C.; Li, J.; Zhang, C.; Tan, Y.; Cheng, J. X. Multiplex Stimulated Raman Scattering Imaging Cytometry Reveals Lipid-Rich Protrusions in Cancer Cells under Stress Condition. *iScience* **2020**, *23* (3), 100953.
(96) Li, J.; Condello, S.; Thomes-Pepin, J.; Ma, X.; Xia, Y.; Hurley, T. D.; Matei, D.; Cheng, J. X. Lipid Desaturation Is a Metabolic Marker and Therapeutic Target of Ovarian Cancer Stem Cells. *Cell Stem Cell* **2017**, *20* (3), 303−314.
(97) Yan, S.; Cui, S.; Ke, K.; Zhao, B.; Liu, X.; Yue, S.; Wang, P. Hyperspectral Stimulated Raman Scattering Microscopy Unravels Aberrant Accumulation of Saturated Fat in Human Liver Cancer. *Anal. Chem.* **2018**, *90* (11), 6362−6366.
(98) Du, J.; Su, Y.; Qian, C.; Yuan, D.; Miao, K.; Lee, D.; Ng, A. H. C.; Wijker, R. S.; Ribas, A.; Levine, R. D.; et al. Raman-guided subcellular pharmaco-metabolomics for metastatic melanoma cells. *Nat. Commun.* **2020**, *11* (1), 4830.
(99) Zhao, G.; Tan, Y.; Cardenas, H.; Vayngart, D.; Wang, Y.; Huang, H.; Keathley, R.; Wei, J. J.; Ferreira, C. R.; Orsulic, S.; et al. Ovarian cancer cell fate regulation by the dynamics between saturated and unsaturated fatty acids. *Proc. Natl. Acad. Sci. U. S. A.* **2022**, *119* (41), No. e2203480119.
(100) Tan, Y.; Li, J.; Zhao, G.; Huang, K. C.; Cardenas, H.; Wang, Y.; Matei, D.; Cheng, J. X. Metabolic reprogramming from glycolysis to fatty acid uptake and beta-oxidation in platinum-resistant cancer cells. *Nat. Commun.* **2022**, *13* (1), 4554.
(101) Vinegoni, C.; Dubach, J. M.; Thurber, G. M.; Miller, M. A.; Mazitschek, R.; Weissleder, R. Advances in measuring single-cell pharmacology in vivo. *Drug Discov Today* **2015**, *20* (9), 1087−1092.
(102) Bazinet, R. P.; Layé, S. Polyunsaturated fatty acids and their metabolites in brain function and disease. *Nat. Rev. Neurosci* **2014**, *15* (12), 771−785.
(103) Martinez-Vicente, M.; Talloczy, Z.; Wong, E.; Tang, G.; Koga, H.; Kaushik, S.; de Vries, R.; Arias, E.; Harris, S.; Sulzer, D.; et al. Cargo recognition failure is responsible for inefficient autophagy in Huntington's disease. *Nat. Neurosci* **2010**, *13* (5), 567−576.
(104) Cole, N. B.; Murphy, D. D.; Grider, T.; Rueter, S.; Brasaemle, D.; Nussbaum, R. L. Lipid droplet binding and oligomerization properties of the Parkinson's disease protein alpha-synuclein. *J. Biol. Chem.* **2002**, *277* (8), 6344−6352.
(105) Welte, M. A. Expanding roles for lipid droplets. *Curr. Biol.* **2015**, *25* (11), R470−481.
(106) Tian, F.; Yang, W.; Mordes, D. A.; Wang, J. Y.; Salameh, J. S.; Mok, J.; Chew, J.; Sharma, A.; Leno-Duran, E.; Suzuki-Uematsu, S.; et al. Monitoring peripheral nerve degeneration in ALS by label-free stimulated Raman scattering imaging. *Nat. Commun.* **2016**, *7*, 13283.
(107) Miao, K.; Wei, L. Live-Cell Imaging and Quantification of PolyQ Aggregates by Stimulated Raman Scattering of Selective Deuterium Labeling. *ACS Cent Sci.* **2020**, *6* (4), 478−486.
(108) Mutlu, A. S.; Gao, S. M.; Zhang, H.; Wang, M. C. Olfactory specificity regulates lipid metabolism through neuroendocrine signaling in Caenorhabditis elegans. *Nat. Commun.* **2020**, *11* (1), 1450.
(109) Zarrouk, A.; Debbabi, M.; Bezine, M.; Karym, E. M.; Badreddine, A.; Rouaud, O.; Moreau, T.; Cherkaoui-Malki, M.; El Ayeb, M.; Nasser, B.; et al. Lipid Biomarkers in Alzheimer's Disease. *Curr. Alzheimer Res.* **2018**, *15* (4), 303−312.
(110) Hong, W.; Karanja, C. W.; Abutaleb, N. S.; Younis, W.; Zhang, X.; Seleem, M. N.; Cheng, J. X. Antibiotic Susceptibility Determination within One Cell Cycle at Single-Bacterium Level by Stimulated Raman Metabolic Imaging. *Anal. Chem.* **2018**, *90* (6), 3737−3743.
(111) Zhang, M.; Hong, W.; Abutaleb, N. S.; Li, J.; Dong, P. T.; Zong, C.; Wang, P.; Seleem, M. N.; Cheng, J. X. Rapid Determination of Antimicrobial Susceptibility by Stimulated Raman Scattering Imaging of D(2)O Metabolic Incorporation in a Single Bacterium. *Adv. Sci. (Weinh)* **2020**, *7* (19), 2001452.
(112) Jusuf, S.; Zhan, Y.; Zhang, M.; Alexander, N. J.; Viens, A.; Mansour, M. K.; Cheng, J. X. Blue Light Deactivation of Catalase Suppresses Candida Hyphae Development Through Lipogenesis Inhibition. *Photochem. Photobiol.* **2022**. DOI: 10.1111/php.13719
(113) Karanja, C. W.; Hong, W.; Younis, W.; Eldesouky, H. E.; Seleem, M. N.; Cheng, J. X. Stimulated Raman Imaging Reveals Aberrant Lipogenesis as a Metabolic Marker for Azole-Resistant Candida albicans. *Anal. Chem.* **2017**, *89* (18), 9822−9829.

(114) Bi, Y.; Yang, C.; Chen, Y.; Yan, S.; Yang, G.; Wu, Y.; Zhang, G.; Wang, P. Near-resonance enhanced label-free stimulated Raman scattering microscopy with spatial resolution near 130 nm. *Light Sci. Appl.* **2018**, *7*, 81.
(115) Saar, B. G.; Freudiger, C. W.; Reichman, J.; Stanley, C. M.; Holtom, G. R.; Xie, X. S. Video-rate molecular imaging in vivo with stimulated Raman scattering. *Science* **2010**, *330* (6009), 1368−1370.
(116) Li, H.; Cheng, Y.; Tang, H.; Bi, Y.; Chen, Y.; Yang, G.; Guo, S.; Tian, S.; Liao, J.; Lv, X.; et al. Imaging Chemical Kinetics of Radical Polymerization with an Ultrafast Coherent Raman Microscope. *Adv. Sci. (Weinh)* **2020**, *7* (10), 1903644.
(117) Zhang, C.; Huang, K.-C.; Rajwa, B.; Li, J.; Yang, S.; Lin, H.; Liao, C.-s.; Eakins, G.; Kuang, S.; Patsekin, V. Stimulated Raman scattering flow cytometry for label-free single-particle analysis. *Optica* **2017**, *4* (1), 103.
(118) Fu, D.; Xie, X. S. Reliable cell segmentation based on spectral phasor analysis of hyperspectral stimulated Raman scattering imaging data. *Anal. Chem.* **2014**, *86* (9), 4115−4119.
(119) Suzuki, Y.; Kobayashi, K.; Wakisaka, Y.; Deng, D.; Tanaka, S.; Huang, C. J.; Lei, C.; Sun, C. W.; Liu, H.; Fujiwaki, Y.; et al. Label-free chemical imaging flow cytometry by high-speed multicolor stimulated Raman scattering. *Proc. Natl. Acad. Sci. U. S. A.* **2019**, *116* (32), 15842−15848.
(120) Nitta, N.; Iino, T.; Isozaki, A.; Yamagishi, M.; Kitahama, Y.; Sakuma, S.; Suzuki, Y.; Tezuka, H.; Oikawa, M.; Arai, F.; et al. Raman image-activated cell sorting. *Nat. Commun.* **2020**, *11* (1), 3452.

https://doi.org/10.1021/acs.jpcb.3c00038
J. Phys. Chem. B 2023, 127, 2381−2394